Defence Technology 13 (2017) 219–227

Contents lists available at ScienceDirect

Defence Technology

journal homepage: www.elsevier.com/locate/dt

Measurement of the spatial specific impulse distribution due to buried high explosive charge detonation

V. Denefeld [a, *], N. Heider [a], A. Holzwarth [b]

[a] Fraunhofer Institute for High-Speed Dynamics, Ernst-Mach-Institut, EMI, Eckerstraße 4, 79104 Freiburg, Germany
[b] Ernst-Mach-Institut, Am Christianswuhr 2, 79400 Kandern, Germany

ARTICLE INFO

Article history:
Received 16 January 2017
Received in revised form
10 March 2017
Accepted 17 March 2017
Available online 28 March 2017

Keywords:
Buried high explosive
IED
Momentum transfer
Specific impulse
Local momentum distribution
Vehicle
Detonation
Ring arrangement setup
Quartz sand
Alluvial sand
Depth of burial
Water content
Saturation
X-ray
High-speed camera

ABSTRACT

Buried high explosive (HE) charges represent a high threat to military vehicles. The detonation of these charges can lead to significant momentum transfer onto vehicles and their occupants. A detailed understanding of the physical processes involved in the loading of vehicle structures is necessary for an optimization of effective countermeasures and protection systems. A quantitative description of the local momentum distribution on the vehicle underbody due to the detonation process is of special importance. In the following, a new test setup is presented that allows the experimental determination of the specific impulse distribution. It is based on a ring arrangement where the elements are nested into each other and the velocity of each ring is correlated with the local specific impulse at its position.

The momentum transfer to a vehicle depends on a number of influencing factors such as: charge mass, embedding material (e.g. sand, gravel, clay), density, water content, saturation, depth of burial, ground clearance and vehicle shape. The presented technology is applied to quantify the influence of the embedding material (alluvial sand, quartz sand), the burial depth and the water content on the local specific impulse distribution. The obtained data can be used as initial condition for the numerical simulation of occupant safety assessment and as input for empirical modeling of momentum transfer on structures.

1. Introduction

Military operations during the last two decades were characterized by asymmetric threat scenarios. Special attention has been given to the effects of land mines and improvised explosive devices (IEDs) on vehicles. A detailed review about anti-tank mines and their effects is given in Ref. [1]. The detonation of mines or IEDs leads to a complex sequence of loading phenomena on vehicle structures. Important effects in this context are the interaction of the blast wave or detonation products with the vehicle as a whole, but also local impacts of primary or secondary fragments onto the vehicle surface. Thus, loading effects can be classified into local and global phenomena. Local effects are related to the impact of projectiles and the development of protective systems with threat adapted material combinations. This paper deals with the physical effects that are caused by the detonation of buried high explosive charges below the military vehicle. In this case, a large momentum transfer on the vehicle structure as a whole takes place and leads to high accelerations of the vehicle and the occupants.

First, most research concentrated on the analysis of low buried mines, and techniques were developed to measure momentum transfer [2,3] and the local deformation of vehicle floor structures [4,5] due to mine detonation. Simulation models for the assessment of mine effects on vehicles were developed [6–8]. Special attention was given to modeling the charge detonation in a sand environment (with adequate material models) and the following interaction with a momentum trapping structure [9,10]. It was realized that the burial conditions and the embedding material properties show a significant influence on the momentum transfer [6,11–16].

* Corresponding author.
E-mail address: vincent.denefeld@emi.fraunhofer.de (V. Denefeld).
Peer review under responsibility of China Ordnance Society.

http://dx.doi.org/10.1016/j.dt.2017.03.002

With the appearance of IEDs, phenomena in connection with deeply buried charges of large masses became of interest [17–19]. It turned out and was partially unexpected that this type of threat caused a significantly increased momentum transfer. Hence, there was the need for a better understanding of this loading process. Influencing factors are: charge mass, embedding material (e.g. sand, gravel, clay), density, water content, saturation, depth of burial, ground clearance and vehicle shape, to mention only the most significant parameters. In most test setups, only the global momentum transfer on a large-area structure was examined. For a better understanding of the loading process, locally resolved information about the specific impulse distribution on a structure is necessary [20–26]. We therefore developed a new test technology based on a ring arrangement with each individual ring used as a momentum trap at the corresponding local position. The HE charge is placed in a barrel structure and embedded within the selected material that is prepared under highly reproducible conditions. After detonation of the charge, the detonation products and the accelerated embedding material interact with the ring arrangement and transfer locally different amounts of impulse on each ring. From the different ring velocities, the corresponding impulse can be derived. For the determination of the ring velocities, redundant measurement techniques are used. In the following, the development of the test design with numerical simulations is shown. The method is used to quantify the influence of several burial parameters on the local momentum distribution. Parameters varied are the embedding material, the water content and the burial depth. The detailed local momentum distribution can be used as initial conditions for numerical simulations of loading processes of vehicles. Additionally, they provide validation material for the empirical description of momentum transfer on structures that is used in several commercial simulation tools.

2. Experimental arrangement

2.1. Description of the experimental setup

In order to characterize the effects of a buried HE charge, most of the tests presented in the literature use large area steel plates as a momentum trap. This approach delivers no information about the spatial momentum distribution. Therefore, a new experimental method has been developed by which the local distribution of the momentum transfer from a HE detonation on a vehicle structure can be obtained. The principle idea is to measure the velocity and thus the momentum transfer of different rigid bodies at different spatial positions that are exposed to the detonation of the buried HE charge. The local specific impulse is determined from the mass, the gained velocity and the surface area of the corresponding body hit by the detonation products. The exposed surface areas of the objects determine the local resolution of the specific impulse measurement.

Our test technology is based on an arrangement with concentric rings where each individual ring is used as a momentum trap at the corresponding local position (see Fig. 1). The arrangement is placed above a sand filled barrel that contains the HE charge. The rings are fixed with wires at the ceiling of the experimental hall and precisely aligned with respect to the sand barrel and its surface.

The ring velocities are determined with redundant measuring techniques: X-ray diagnostic and high-speed camera.

The experimental setup is shown in Fig. 1. The explosive charge is embedded in an accurately prepared sand environment. The sand barrel has a diameter of 63 cm and a height of 80 cm, which is replaced for each test and is filled with sand again.

2.2. Charge definition

A PETN charge (with a density of 1.54 g/cm^3) has a mass of 84 g with a diameter of 59.2 mm. The depth of burial of the explosive charge (distance from the top of the charge to the top of the soil) varies from 46.4 mm to 116 mm. The initiation of the charge occurs at the center of the bottom of the explosive charge. The distance between the sand surface and the ring structure is 139 mm.

2.3. Sand definition

A defined and reproducible preparation of the embedding material is of great importance. For our tests we used loose sand material which is a heterogeneous material consisting of the quartzite grains, water and the air voids. The effects of buried HE charges depend strongly on the actual composition between these three components. It is therefore necessary to prepare a largely homogeneous mixture of the components within the test barrel. Special attention was given to an exact determination of the water content and the water saturation. The intention was to determine the local momentum distribution as a function of these parameters.

Two different sand types have been chosen for the experiments: an alluvial sand, with 5% water content, and a dry quartz sand. The grain size distributions for the materials are shown in Fig. 2. It can be seen that 80% of the sand particles have a size between 0.1 mm and 0.3 mm which corresponds to a rather fine-grained particle distribution.

As mentioned before, the two parameters water content and the saturation are of special importance for the preparation of defined test conditions. Both parameters have to be prepared in the sand barrel as homogeneous as possible connected with a precise experimental determination of their actual values at the time of testing.

Therefore, we determined the following parameters for each experiment: wet density ρ_{wet}, water content w, dry density ρ_{dry} and saturation S. In the following we give a short summary of the measurements and formulae used for the determination of these parameters.

Shortly before the test, the selected amount of water and sand was mixed and evenly distributed in the test barrel. Afterwards, sand samples (with mass m_{sample}) were taken from the prepared sand in the test barrel with help of a core cutter (height 120 mm, diameter 96 mm, volume $V_{\mathrm{sample}} = 868$ mm^3).

The wet sand density ρ_{wet} results from Equ.1

$$\rho_{\mathrm{wet}} = \frac{m_{\mathrm{sample}}}{V_{\mathrm{sample}}} \tag{1}$$

The taken sand sample is then heated at a temperature of 105 °C until the complete water fraction has disappeared from the sample. The sand sample is then weighed and the mass of the dry sand m_{dry} is determined.

The water content w is calculated from Equ.2

$$w = \frac{m_{\mathrm{water}}}{m_{\mathrm{dry}}} \tag{2}$$

with m_{water} being the evaporated water mass.

The dry density ρ_{dry} is calculated from Equ.3

$$\rho_{\mathrm{dry}} = \frac{\rho_{\mathrm{wet}}}{1+w} \tag{3}$$

which finally gives the saturation ratio S with Equ.4

Fig. 1. Measurement setup with concentric rings suspended at wire cables (left), screw connection of the wire cables at the rings (right).

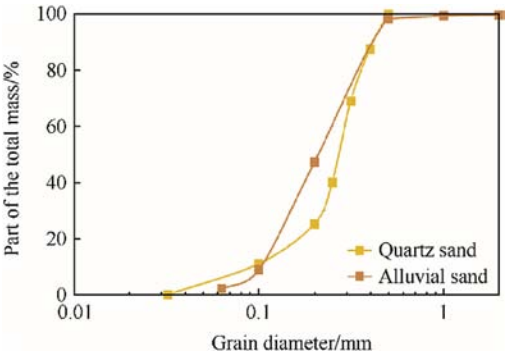

Fig. 2. Grain size distribution for quartz sand and alluvial sand.

$$S = \frac{w \times \rho_{\text{dry}}}{\rho_{\text{water}} \times \left(1 - \frac{\rho_{\text{dry}}}{\rho_s}\right)} \tag{4}$$

where ρ_s is the density of the single quartz grain which has a value of $\rho_s = 2.65$ g/cm^3.

3. Design of the rings

The design of ring shapes requires a detailed analysis of the expected initial velocities and trajectories of each individual ring element. This is of special importance for the X-ray and optical measurement of the ring velocities. An unambiguous allocation of the rings is only possible if overlapping of the inner rings by outer rings can be avoided. In order to ensure that the rings will be visible on X-ray pictures, the heights of the rings have to be optimized with the help of numerical simulations. For example, if an outer ring would fly faster than the inner rings, these rings would be covered and not observable on the X-ray picture anymore. A variation of the geometry of the ring shape has been done to achieve an optimal velocity for each ring.

To avoid contact of the flying rings with the ceiling of the experimental hall, a certain initial velocity must not be exceeded. For our test conditions the maximum flight height should be less than 3 m which corresponds to a maximum initial velocity of less than 7.7 m/s.

The selected ring configuration is presented in Fig. 3. It consists in 8 concentric rings with a thickness of 20 mm and with heights ranging from 60 mm to 140 mm. The total weight of the rings is 57 kg. Special attention has been devoted to the choice of an

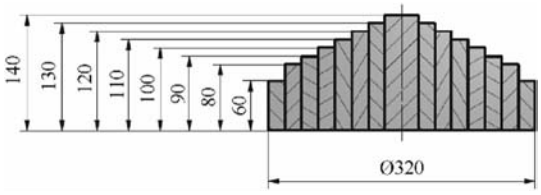

Fig. 3. Drawing of the ring configuration.

appropriate gap size between the rings of 0.2 mm, small enough to prevent that sand fills the gap, and large enough to minimize friction. On top of that, oil has been added between the rings and it has been checked before each experiment that the rings could slide between them.

4. Diagnostic methods

In order to calculate the specific impulse, an accurate measurement of the initial ring velocity is necessary. For the diagnostic, a 3-channel X-ray flash unit and a high-speed camera are used to measure the velocity of the rings. Fig. 4 shows an overall view of the experimental setup as created at the test facility. An X-ray film and

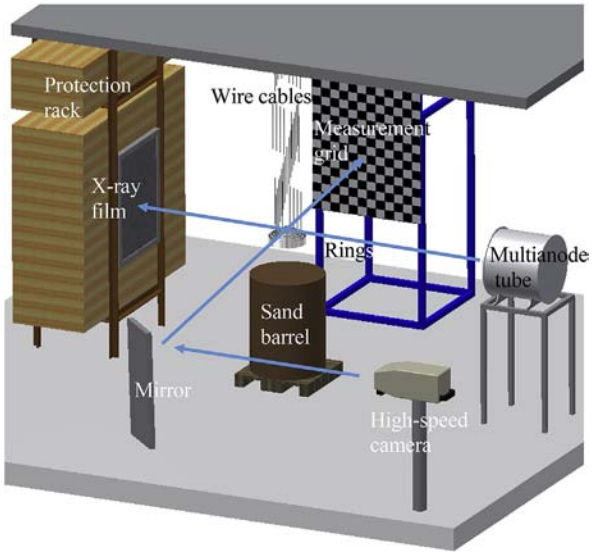

Fig. 4. Overall view of the test setup.

a measurement grid for the determination of the ring displacement are located behind the sand barrel. A 3-channel X-ray source (multianode tube) for the production of the X-ray flash pictures can be seen on the right. The sand barrel is located in the center of the picture, with concentric rings for the impulse measurement. On the left, wooden blocks are placed for protection against fragments.

For the X-ray analysis, the flight height and the trigger times are determined with the numerical simulation. The velocity of the rings during their rising phase is presented in Fig. 5 for a depth of burial of 46.4 mm.

Using X-ray diagnostics, two or three images are taken after the initiation of the charge. With numerical simulations, it has been showed that the impulse is completely transferred onto the rings after about 2 ms. The determination of the initial velocity of the rings should therefore start after 2 ms in order to prevent disturbing influences from the acceleration phase. As a consequence, the trigger time of the first X-ray picture will be set 2 ms after the initiation of the explosive."

Initial velocity values v_0 can easily be determined from the path and time differences between two X-ray pictures. An example of two X-ray pictures is given in Fig. 6. If s_1 and s_2 are the positions of the rings at the corresponding recording times t_1, t_2, v_0 results from Equ. 5

$$v_0 = \frac{(s_2 - s_1) + \frac{1}{2}g(t_2^2 - t_1^2)}{t_2 - t_1} \quad (5)$$

with $g = 9.81\ m/s^2$ the acceleration due to gravity.

The specific impulses i_S transferred to the rings are then calculated using Equ. 6

$$i_S = \frac{m \times v_0}{F} \quad (6)$$

with m the mass of the ring and F the annular surface, $[i_S] = [kg/m \cdot s] = [Pa \cdot s]$.

Another method to evaluate the initial velocity of the rings is the use of the high-speed video.

The video films cover the entire flight phase of the rings over a period of 2000 ms. The detonation flash and the sand particles make the evaluation of the velocity of the rings in the first milliseconds of the video very difficult. The cases in which the rings are observable when they fall back to the starting position (see, for example, Fig. 7) can nevertheless be used to calculate the transferred impulse from the flight time. In this case, the initial velocity v_0 is given by Equ. 7

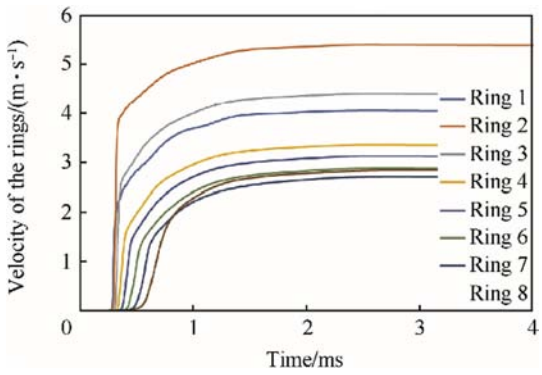

Fig. 5. Acceleration phase of the rings 1 to 8 (1 being central) as a function of the time, for the depth of burial 46.4 mm, calculated with the numerical simulation.

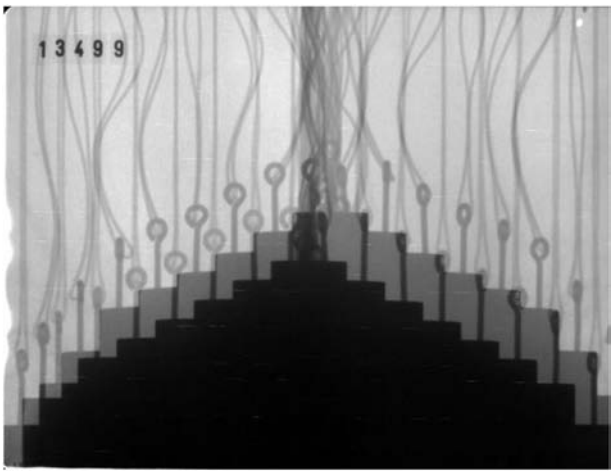

Fig. 6. X-ray film of test No. 8 (trigger times: $t_1 = 2$ ms, $t_2 = 8$ ms).

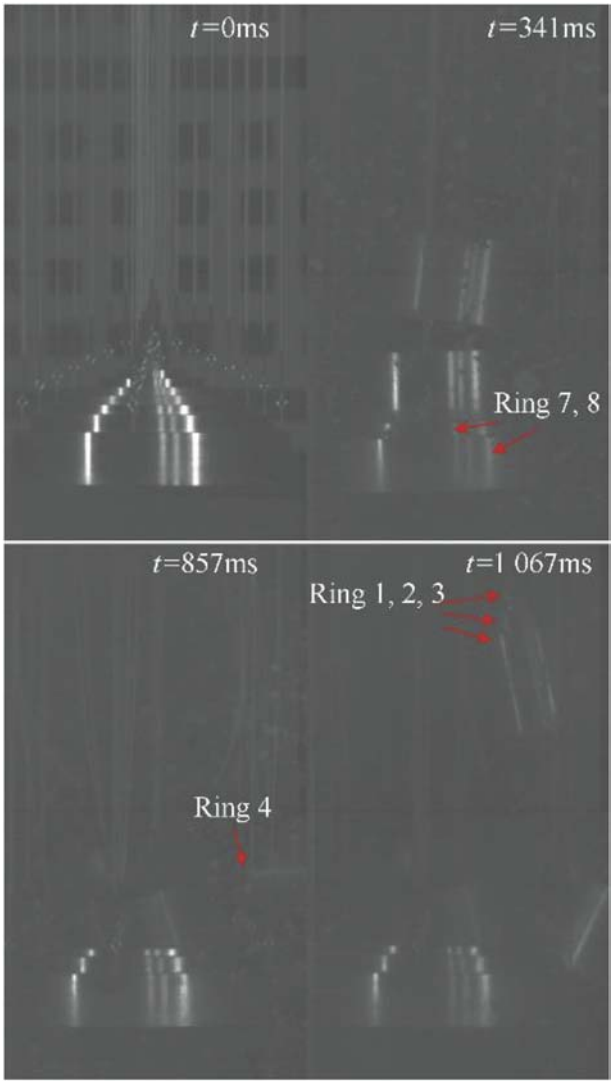

Fig. 7. Position of the rings at $t = 0$, 341, 857 and 1067 ms for the calculation of the initial velocities (test No. 2).

$$v_0 = \frac{t_f \times g}{2} \quad (7)$$

with the flight time t_f and the gravitational constant $g = 9.81\ m/s^2$.

A comparison of the initial velocity determined by the two methods is given for test No. 2 in Table 1. The ring No. 5 is not discernable on the high-speed video.

Regarding the measurement accuracy, the two experimental methods for the determination of the ring velocities are in good agreement. The evaluation of the ring velocity using X-ray diagnostics, however, proves to be more reliable and will be preferred in the following.

5. Experimental measurement of the spatial specific impulse distribution

In the following, the experimentally determined spatial specific impulse distributions are presented. Table 2 shows an overview of the 10 experiments including the performed variation of the burial conditions. Experiments 1 to 4 were carried out with alluvial sand, Experiments 6 to 10 with quartz sand. The depth of burial was chosen to be 46.4 mm and 116 mm for alluvial sand and 46.4 mm for quartz sand. The variation of water content and saturation was done for quartz sand (water content between 0 and 20% and saturation between 6% and 67%).

Experiment results showing the specific impulse as a function of the radial distance are shown in Fig. 8 for the alluvial sand. The error bars correspond to the maximum and minimum value in the two tests with similar embedding conditions. The comparison of the results for the 2 different burial depths shows the interesting fact that the specific impulse distribution is more concentrated to small radial distances for the higher burial depth. Up to the radial distance of 70 mm, the test with a depth of 116 mm shows significantly higher impulse values. Going to larger radial distances (90 mm and more), the shallow buried charge causes the larger momentum transfer to the structure. The physical explanation is quite intuitive because the deeper buried charge is more contained by the surrounding material and thus the detonation products are directed more perpendicularly and concentrated with respect to the embedding material surface. It is remarkable that the total momentum transfer integrated over the complete loaded area is nearly identical for both burial depths (see Fig. 9, with a maximum value of 174 kg·m/s after integration over the complete loaded area). This demonstrates that the loading of a vehicle due to a buried charge detonation depends sensitively on the burial depth but also on the vehicle area that collects the ejected ground material. An exact quantification of the loading conditions thus requires the detailed knowledge of the spatial specific impulse distribution with respect to the vehicle ground floor.

The corresponding results for the quartz sand are shown in Fig. 10. For this material, a systematic variation of the water content and saturation has been done. The corresponding results for the specific impulse are shown in this case as a function of the radial distance and the degree of saturation. Saturation values are 0%, 32% and 66%. It is found that the scattering of the experimental results is quite small and thus a reproducible preparation of the soil has been achieved. Surprisingly it can be observed that directly over the mine, the dry sand causes higher specific impulse than the wet sand. For some radial distances up to 90 mm there is nearly a factor of 2 between dry and wet sand. For larger distances, wet sand shows significantly higher specific impulse values. Remarkable is the fact that the experiments with water saturation of 32% and 66% show nearly no difference within the experimental error. It is again interesting to look at the total integrated momentum in Fig. 11, and at the summary for all sand configurations in Fig. 12. The cumulative integrated impulse as a function of radial distance shows again the higher values for the dry sand but with increasing radial distance, dry sand and wet sand show a converging behavior. The total momentum integrated over the complete loaded area for the dry sand (value of 242 kg·m/s) leads only to a slightly higher momentum transfer of around 14% compared with the wet sand (about 213 kg·m/s). The total momentum transfer for the 32% and 66% saturation is identical and shows no further dependence on this parameter. Our experimental results do not support a significant effect of saturation in the parameter field that we investigated.

Table 1
Determination of initial velocity of the rings for test No. 2.

Ring No.	v_0 (using video)/(m·s^{-1})	v_0 (using X-ray diagnostics)/(m·s^{-1})
1, 2, 3	5,62	6,03
4	4,20	4,50
5	–	2,67
6, 7, 8	1,62	1,75

6. Numerical simulation

6.1. Variation of the depth of burial of the charge

For a detailed analysis of the experimental results, simulation models of the test setup have been developed. The concentric ring arrangement shows rotational symmetry and therefore allows 2D as well as 3D finite element simulations. The 3D numerical simulation model is shown in Fig. 13. Simulations are executed with the finite-element software LS-DYNA. The rings are represented by a Lagrange model (32 000 solid elements), the embedding material with the HE charge and the surrounding air are represented by an Euler model (1.4 million solid elements). The detonation process is simulated with a complete Euler-Lagrange coupling method. Special attention must be addressed to the material modeling of the sand material. The model from Laine and Sandvik [9] for sand was used, which includes an equation of state for the compaction of loose sand particles and a Mohr-Coulomb type model for the strength behavior. The initial density of the sand was set to 1,3 g/cm^3 by scaling the equation of state of the model of Laine and Sandvik.

The depth of burial of the charge was varied from 23.2 mm to 116 mm. The specific impulse and the maximal velocity of the rings are shown in Fig. 14 and Fig. 15, respectively.

The momentum transferred to the rings is concentrated within a circular area of about 15 cm radius. The maximal velocity of the ring is about 6 m/s, and the maximal flight height about 1.8 m, meeting the requirement of the testing facility.

It can be observed that the impulse is focused directly above the charge for small depths of burial. For more deeply buried charges, the impulse is transferred outwards.

6.2. Comparison with experiments and extension of the model

Special attention has been devoted to validate the material model and to increase the lateral extension of the observation range. In the experiments, the radius of the ring arrangement is 160 mm and part of ejected material and thus momentum will pass the test setup. Numerical simulations provide the information about the momentum that is not detected in the experiment. The simulation model with an extended 600 mm momentum trap configuration is presented in Fig. 16.

The numerical simulations are validated and compared with the experiments 3 and 4 (alluvial sand, depth of burial 46.4 mm) where

Table 2
List of the experiments with prepared burial conditions.

Test No.	Soil type	Depth of burial/mm	Wet density/(g·cm^{-3})	Water content/%	Saturation/%
1	Alluvial sand	116	1.59	3.8	8.8
2	Alluvial sand	116	1.25	5.5	9.5
3	Alluvial sand	46.4	1.27	3.8	6.7
4	Alluvial sand	46.4	1.25	7.2	12
5	Quartz sand	46.4	1.60	0	0
6	Quartz sand	46.4	1.60	0	0
7	Quartz sand	46.4	1.59	10	31.6
8	Quartz sand	46.4	1.59	10	31.6
9	Quartz sand	46.4	1.77	20	66.8
10	Quartz sand	46.4	1.80	17.8	64.7

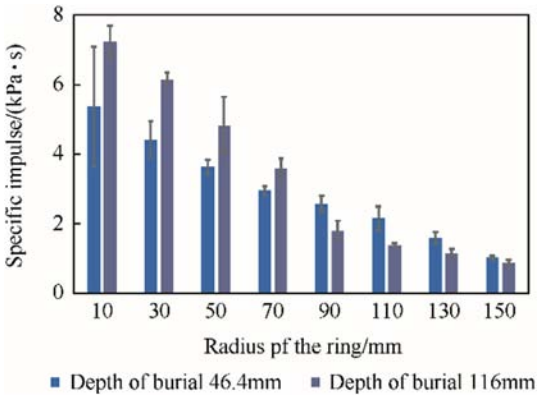

Fig. 8. Spatial specific impulse distribution for alluvial sand.

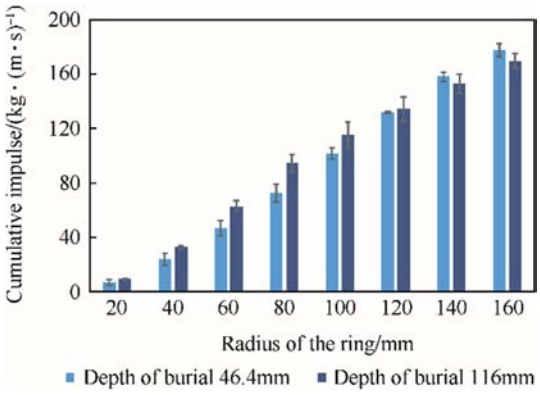

Fig. 9. Cumulative impulse distribution for alluvial sand.

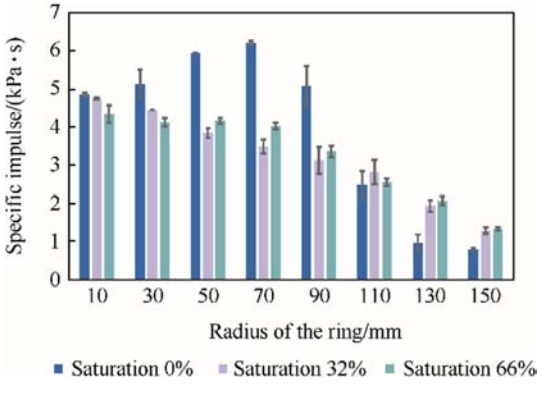

Fig. 10. Spatial specific impulse distribution for quartz sand (depth of burial 46.4 mm).

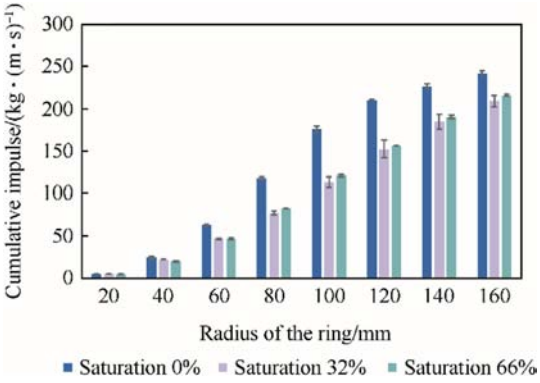

Fig. 11. Cumulative impulse distribution for quartz sand (depth of burial 46.4 mm).

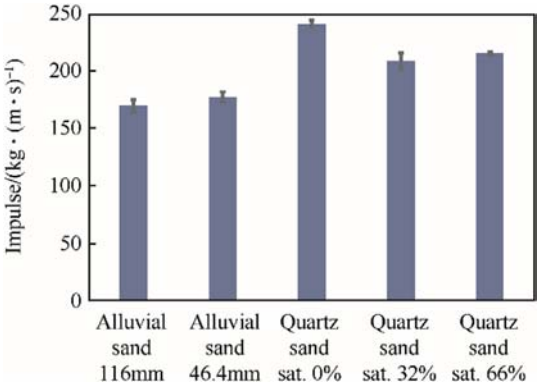

Fig. 12. Total momentum integrated over the loaded area for different burial conditions.

the prepared test conditions match with material parameters of our selected material model.

The specific impulse distributions from Experiment 3 and 4 are compared with the numerical simulation in Fig. 17. The integrated cumulative momentum is shown in Fig. 18. Regarding the specific impulse, the simulation values are ranging from 5.5 kPa·s in the center region to 1.3 kPa·s for the maximum observed radial distance. The corresponding average test values are in the range from 5.4 kPa·s for the first ring to 1.1 kPa·s for the outer ring. Regarding the cumulative impulse distribution, the average total momentum integrated over the complete loaded area for Tests 3 and 4 is 178 kg·m/s. The total momentum calculated with the numerical simulation is 187 kg·m/s, within 5% from the average total momentum of the experiments. Overall, a good agreement between numerical simulation and the experiments is observed.

Another method to quantify the specific impulse distribution is

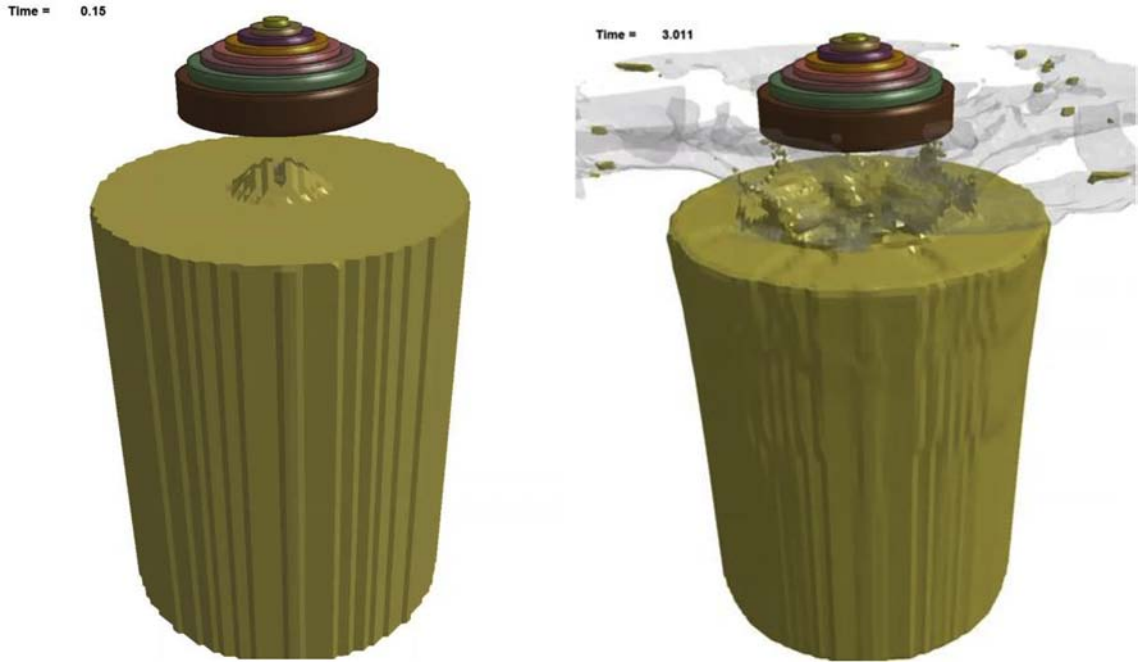

Fig. 13. Simulation model 150 μs (left) and 3 ms (right) after detonation.

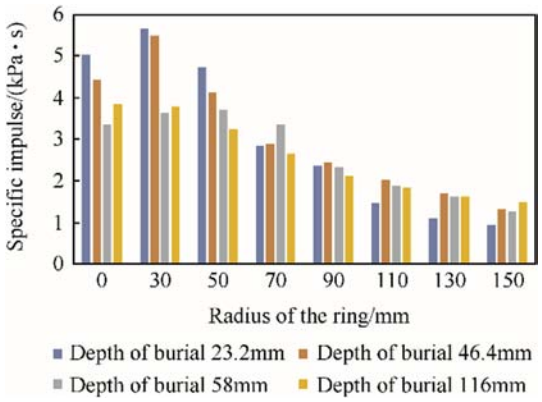

Fig. 14. Simulation of the specific impulse as a function of the radial distance (depth of burial variation).

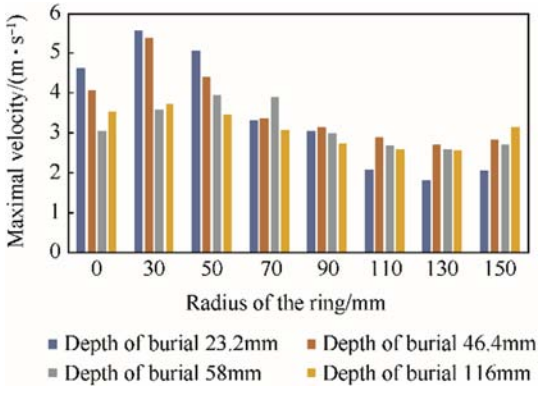

Fig. 15. Maximal velocity as a function of the radius of the ring according to numerical simulation. Variation of the depth of burial.

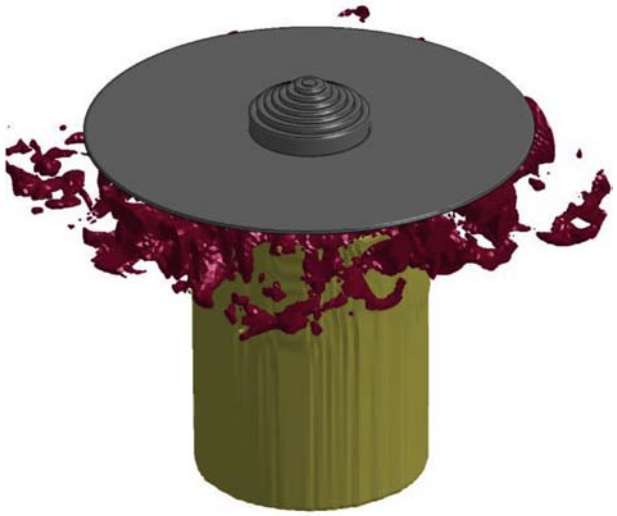

Fig. 16. Simulation model with the additional momentum trap of 600 mm radius (alluvial sand, depth of burial 46.4 mm, time $t = 4.2$ ms).

based on the work of Westine (see Refs. [27] and [28]). Westine conducted experiments with buried explosives in soil. He then used an analytical empirical approach to postulate a formula where the local distribution of the specific impulse on a flat plate is given as a function of the configuration (mass, energy and geometry of the explosive, burial depth, distance to the plate). The functional dependence of the specific impulse on the radial distance resembles the shape of a Gaussian bell curve with a strong decrease with increasing radial distance to the charge center. The corresponding specific momentum distribution calculated from the Westine formula is compared with our experimental results and our simulation and is shown in Fig. 17. It is obvious that the analytical formula overestimates the experiments by about 50% and thus can be used only for a rough estimate of buried charge

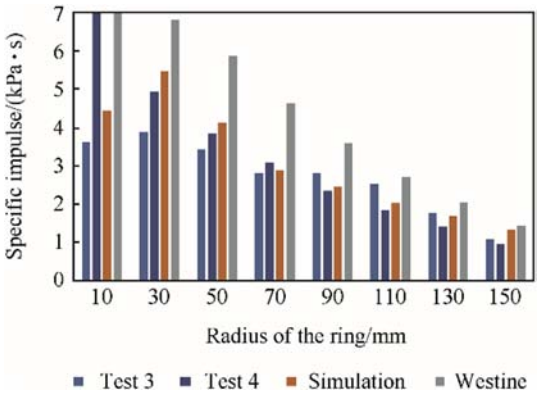

Fig. 17. Comparison between experiment and simulation, specific impulse distribution (Tests 3 and 4, alluvial sand, depth of burial of 46.4 mm).

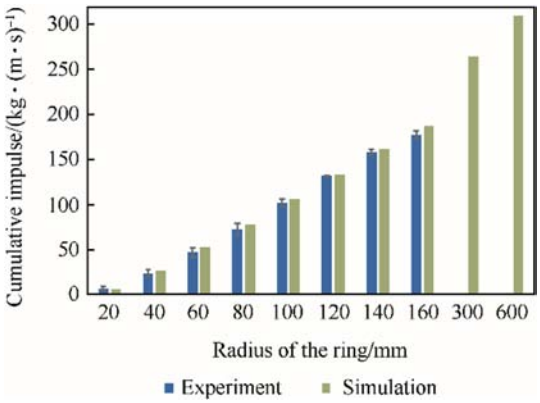

Fig. 18. Comparison between experiment and simulation with the momentum trap, cumulative impulse (Tests 3 and 4, alluvial sand, depth of burial of 46.4 mm).

detonation effects.

The cumulative impulse distribution calculated with the additional momentum traps of 300 and 600 mm radius (Fig. 19) shows that the cumulative impulse still increases with increasing ring radius, with values of 265 kg·m/s at a radius of 300 mm and of 310 kg·m/s at a radius of 600 mm. The total momentum trapped by the tested configuration (160 mm ring radius) corresponds to about 60% of the total momentum that would have been trapped with the 600 mm ring radius. It can be supposed that for our burial condition and a radius of the momentum trap from 600 mm, the total momentum of the explosive charge and of the sand has been transferred.

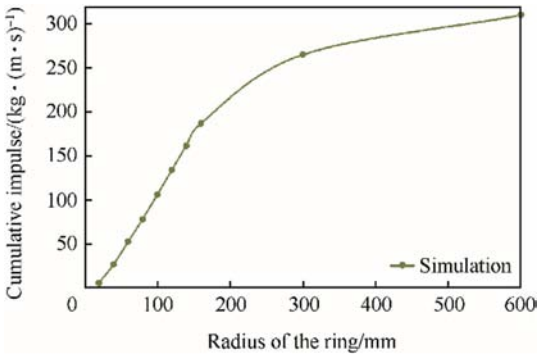

Fig. 19. Cumulative impulse distribution for the simulation with the momentum trap (alluvial sand, depth of burial of 46.4 mm).

7. Summary

A measurement technique was presented that allows the experimental determination of the local specific impulse distribution of a buried HE charge detonation. The test setup was designed and optimized with numerical simulations. An arrangement of concentric rings where the individual rings are nested into each other was found to be particularly suitable for specific impulse measurement. The vertical ring velocities were measured and correlated with the transmitted specific impulse. X-ray imaging and high-speed video recordings were used to measure the ring velocities. The different diagnostic tools that were used gave very consistent results for the measured rings velocities and thus for the local specific impulse.

1)The presented method was used to quantify the influence of the following burial conditions on the local specific impulse distribution: variation of embedding material (alluvial sand, quartz sand), depth of burial, water content and saturation. A very defined and reproducible preparation of the embedding test bed was given special attention. This is a requirement for a correct assessment of important influencing factors for the momentum transfer.

2)For the embedding material alluvial sand, the specific impulse shows a distribution as function of the radial distance that resembles a Gaussian bell shape curve. The maximum specific impulse directly above the charge is 8 kPa·s and decays to a value of 4 kPa·s within a radial distance of 70 mm.

3)For the embedding material quartz sand, the radial distribution of the specific impulse is broadened compared to alluvial sand with the highest value of 6 kPa·s at a radial distance of 70 mm. The specific impulse directly above the charge shows lower values around 5 kPa·s.

4)There is no clear dependency of the momentum transfer on the saturation. When the charge is embedded in quartz sand, the specific impulses are higher for the completely dry sand in the area above the charge than with saturation 32% and 66%. However, the two cases with a higher water content only differ slightly among each other. The experimental results can be used as a database for the development of numerical simulation models and the improvement of empirical momentum transfer models.

Acknowledgments

The authors want to thank TRDir K. Hüsing from the German test range WTD-91 GF-440 in Meppen and TRDir K. Neugebauer from BAAINBw for funding this work.

References

[1] Showichen A. Numerical analysis of vehicle bottom structures subjected to anti-tank mine explosions. Cranfield University; 2008. PhD thesis, https://dspace.lib.cranfield.ac.uk/bitstream/1826/2914/1/showichen_final_100708.pdf.
[2] Grujicic M, et al. Impulse loading resulting from shallow buried explosives in water-saturated sand. Proc IMechE 2007;221(Part I):21–34.
[3] Bergeron DM, Tremblay JE. Canadian research to characterize mine blast output, vol. 16. Oxford: MABS; 2000.
[4] Neuberger A, Peles S, Rittel D. Scaling the response of circular plates subjected to loarge and close-range spherical explosions. Int J Impact Eng 2007;34:874–82.
[5] Zakrisson B. Numerical simulations of blast loaded steel plates for improved vehicle protection. Lulea University of Technology; 2013. PhD thesis, http://ltu.diva-portal.org/smash/get/diva2:999223/FULLTEXT01.pdf.
[6] Fiserova D. Numerical analyses of buried mine explosions with emphasis on

effect of soil properties on loading. Cranfield University; 2006. PhD Thesis, https://dspace.lib.cranfield.ac.uk/bitstream/1826/1209/1/darina%2520fiserova.pdf.
[7] Williams K, McClennan S, Durocher R, St-Jean B, Tremblay J. Validation of a loading model for simulating blast mine effects on armoured vehicles. 2009.
[8] Borvik T, Olovsson L, Hanssen AG, Dharmasena KP, Hansson H, Wadley H. A discrete particle approach to simulate the combined effect of blast and sand impact loading of steel plates. J Mech Phys Solids 2011;59:940–58.
[9] Laine L, Sandvik A. Derivation of mechanical properties for sand. In: Proceedings of the 4th asia-pacific conference on shock and impact loads on structures. Singapore: CI-Premier PTE LTD; 2001.
[10] Heider N, Klomfass A. Numerical and experimental analysis of the detonation of sand-buried mines. In: 22nd international symposium on ballistics; 2005. Vancouver.
[11] Anderson Jr CE, Behner T, Weiss CE. Mine blast loading experiments. Int J Impact Eng 2011;(38):697–706.
[12] Heider N, Denefeld V, Holzwarth A. Methods for the analysis of global IED effects on military vehicles. In: European survivability workshop; 2010. Alesund, Norway.
[13] Clarke S, Fay S, Warren J, Tyas A, Rigby S, Reay J, Livesey R, Elgy I. Geotechnical causes for variations in output measured from shallow buried charges. Int J Impact Eng 2015;86:274–83.
[14] Clarke S, Fay S, Warren J, Tyas A, Rigby S, Reay J, Livesey R, Elgy I. Predicting the role of geotechnical parameters on the output from shallowed buried explosives. Int J Impact Eng 2017;102:117–28.
[15] Fox D, Lee J. The influence of water, dry sand, and unsaturated sand constitutive behavior on the blast response of a rigid target. Int J Impact Eng 2014;65:163–73.
[16] McShane G, Deshpande V, Fleck N. A laboratory-scale buried charge simulator. Int J Impact Eng 2013;62:210–8.
[17] Heider N, Denefeld V, Holzwarth A, Sättler A, Salk M. Vehicle protection against global IED effects. In: 27th international symposium on ballistics; 2013. Freiburg.
[18] Denefeld V, Heider N, Holzwarth A, Sättler A, Salk M. Reduction of global effects on vehicles after IED detonations. In: 28th international symposium on ballistics; 2014. Atlanta.
[19] Heider N, Denefeld V, Steinbrenner A, Holzwarth A. Engineering tool for the evaluation of global IED effects. In: 29th international symposium on ballistics; 2016. Edinburgh.
[20] Wenzel AB, Esparza ED. Measurements of pressures and impulses at close distances from explosive charges buried and in air. 1972. SwRI-Report.
[21] Held M. Blast effects with the held momentum method. In: 21st international symposium on ballistics; 2004. Adelaide.
[22] Assaf A, et al. The influence of soil conditions on the blast intensity for sand, clayey sand and gravel with silt. In: 28th international symposium on ballistics; 2014. Atlanta, GA, USA.
[23] Rigby S, Fay S, Clarke S, Tyas A, Reay J, Warren J, Gant M, Elgy I. Measuring spatial pressure distribution from explosives buried in dry Leighton Buzzard sand. Int J Impact Eng 2016;96:89–104.
[24] Clarke S, Fay S, Warren J, Tyas A, Rigby S, Elgy I. A large scale experimental approach to th measurement of spatially and temporally localised loading from the detonation of shallow-buried explosives. Meas Sci Technol 2015;26:015001.
[25] Zhao X, Tiwari V, Sutton M, Deng X, Fourney WL, Leiste U. Scaling of the deformation histories for clamped circular plates subjected to blast loading by buried charges. Int J Impact Eng 2013;54:31–50.
[26] Mullin S, Carpenter AJ, Riegel III JP, Cox PA, McFarland JM, Weiss C, Walker JD, Riha DS, Grosch DJ, Mathis JT. New analytical formulations for land minde total and specific impulse predictions. In: 28th internation symposium on ballistics; 2014. Atlanta.
[27] Westine P, Morris BL, Cox PA, Polch EZ. Development of computer program for floor plate response from land explosions. 1985.
[28] Tremblay J. Impulse on blast deflectors from a landmine explosion. Valcartier, Canada: Defence research establishement; 1998.